AFRL-RZ-WP-TP-2010-2243

HYDROCARBON-FUELED SCRAMJET COMBUSTOR FLOWPATH DEVELOPMENT FOR MACH 6-8 HIFiRE FLIGHT EXPERIMENTS (PREPRINT)

Mark R. Gruber and Kevin Jackson

Propulsion Sciences Branch
Aerospace Propulsion Division

Jiwen Liu

Taitech, Inc.

MAY 2008

AIR FORCE RESEARCH LABORATORY
PROPULSION DIRECTORATE
WRIGHT-PATTERSON AIR FORCE BASE, OH 45433-7251
AIR FORCE MATERIEL COMMAND
UNITED STATES AIR FORCE

REPORT DOCUMENTATION PAGE

Form Approved
OMB No. 0704-0188

1. REPORT DATE *(DD-MM-YY)*	2. REPORT TYPE	3. DATES COVERED *(From - To)*
May 2008	Conference Paper Preprint	01 August 2007 – 31 May 2008

4. TITLE AND SUBTITLE
HYDROCARBON-FUELED SCRAMJET COMBUSTOR FLOWPATH DEVELOPMENT FOR MACH 6-8 HIFiRE FLIGHT EXPERIMENTS (PREPRINT)

5a. CONTRACT NUMBER
In-house

5b. GRANT NUMBER

5c. PROGRAM ELEMENT NUMBER
62203F

6. AUTHOR(S)
Mark R. Gruber and Kevin Jackson (AFRL/RZAS)
Jiwen Liu (Taitech, Inc.)

5d. PROJECT NUMBER
3012

5e. TASK NUMBER
AI

5f. WORK UNIT NUMBER
3012AI00

7. PERFORMING ORGANIZATION NAME(S) AND ADDRESS(ES)
Propulsion Sciences Branch (AFRL/RZAS)
Aerospace Propulsion Division
Air Force Research Laboratory, Propulsion Directorate
Wright-Patterson Air Force Base, OH 45433-7251
Air Force Materiel Command, United States Air Force

Taitech, Inc.
1430 Oak Court, Suite 301
Beavercreek, OH 45430

8. PERFORMING ORGANIZATION REPORT NUMBER
AFRL-RZ-WP-TP-2010-2243

9. SPONSORING/MONITORING AGENCY NAME(S) AND ADDRESS(ES)
Air Force Research Laboratory
Propulsion Directorate
Wright-Patterson Air Force Base, OH 45433-7251
Air Force Materiel Command
United States Air Force

10. SPONSORING/MONITORING AGENCY ACRONYM(S)
AFRL/RZAS

11. SPONSORING/MONITORING AGENCY REPORT NUMBER(S)
AFRL-RZ-WP-TP-2010-2243

12. DISTRIBUTION/AVAILABILITY STATEMENT
Approved for public release; distribution unlimited.

13. SUPPLEMENTARY NOTES
Paper presented at the JANNAF Joint Subcommittee Meeting, meeting held May 12 – 16, 2008 in Newton, MA. This paper contains color. PA Case Number: WPAFB 08-3167; Clearance Date: 06 May 2008.

14. ABSTRACT
The Hypersonic International Flight Research Experimentation (HIFiRE) Program is a joint effort between the US Air Force Research Laboratory (AFRL) and the Australian Defence Scientific and Technology Organisation (DSTO) devoted to the study of basic hypersonic phenomena through flight experimentation. Experiments have been planned to explore the operating, performance, and stability characteristics of a simple hydrocarbon-fueled scramjet combustor as it transitions from dual-mode to scramjet-mode operation and during supersonic combustion at Mach 8+ flight conditions. This paper describes initial efforts to develop the isolator/combustor flowpath for these flight experiments. Computational results suggest that excellent performance can be obtained at Mach 8 flight conditions with simple inclined wall fuel injection upstream of a cavity-based flameholder using both ethylene and a mixture of ethylene and methane. Computational analyses have also been used to explore combustor operability and performance at flight Mach numbers between 6 and 8 to identify where mode transition can be expected to occur.

15. SUBJECT TERMS
supersonic combustion, flight experimentation, CFD

16. SECURITY CLASSIFICATION OF:			17. LIMITATION OF ABSTRACT:	18. NUMBER OF PAGES	19a. NAME OF RESPONSIBLE PERSON (Monitor)
a. REPORT	b. ABSTRACT	c. THIS PAGE			Mark R. Gruber
Unclassified	Unclassified	Unclassified	SAR	22	19b. TELEPHONE NUMBER *(Include Area Code)* N/A

Standard Form 298 (Rev. 8-98)
Prescribed by ANSI Std. Z39-18

HYDROCARBON-FUELED SCRAMJET COMBUSTOR FLOWPATH DEVELOPMENT FOR MACH 6-8 HIFIRE FLIGHT EXPERIMENTS

Mark Gruber,* Kevin Jackson,† and Thomas Jackson‡
Air Force Research Laboratory, Propulsion Directorate
Wright-Patterson AFB, OH 45433

Jiwen Liu§
Taitech, Inc.
Beavercreek, OH 45430

ABSTRACT

The Hypersonic International Flight Research Experimentation (HIFiRE) Program is a joint effort between the US Air Force Research Laboratory (AFRL) and the Australian Defence Scientific and Technology Organisation (DSTO) devoted to the study of basic hypersonic phenomena through flight experimentation. As part of this multi-flight program, experiments have been planned to explore the operating, performance, and stability characteristics of a simple hydrocarbon-fueled scramjet combustor as it transitions from dual-mode to scramjet-mode operation and during supersonic combustion at Mach 8+ flight conditions. This paper describes initial efforts to develop the isolator/combustor flowpath for these flight experiments. To date, computational results suggest that excellent performance can be obtained at Mach 8 flight conditions with simple inclined wall fuel injection upstream of a cavity-based flameholder using both ethylene and a mixture of ethylene and methane. The fuel mixture is intended to simulate partially-cracked JP7. In addition, computational analyses have been used to explore combustor operability and performance at flight Mach numbers between 6 and 8 to identify where the transition from dual-mode to scramjet-mode operation can be expected to occur.

NOMENCLATURE

A	=	area
E	=	integrated energy flow
h	=	flowpath height, enthalpy
k	=	turbulent kinetic energy
KE	=	integrated kinetic energy flow
mom_i	=	integrated momentum flow components
M	=	Mach number
P	=	pressure
Pr_t	=	turbulent Prandtl number
Q	=	dynamic pressure
Sc_t	=	turbulent Schmidt number
T	=	temperature
u_i	=	velocity components
V	=	velocity
V_c	=	velocity correction term
W	=	mass flow rate
x	=	axial coordinate relative to isolator entrance
y	=	transverse coordinate relative to cowl wall or combustor mid-plane

* Senior Aerospace Engineer.
† Aerospace Engineer.
‡ Deputy for Science.
§ Senior Research Scientist.

z	=	spanwise coordinate
Y_i	=	species mass fraction
α	=	angle of attack
β	=	combustor divergence angle
ε	=	dissipation
ϕ	=	equivalence ratio
ϕ_B	=	burned equivalence ratio = $\phi * \eta_c$
η_a	=	area correction term
η_c	=	combustion efficiency
ρ	=	density
ω	=	turbulent frequency

Subscripts

ideal	=	ideal condition
ref	=	reference condition
x, y, z	=	coordinate directions
0	=	freestream
2	=	isolator entrance station
4	=	combustor exit station

INTRODUCTION

Hydrocarbon-fueled scramjet combustors have been extensively studied in ground-based facilities over a range of test conditions simulating flight from Mach 4 to 6.5, while a limited number of efforts have explored combustor operation above Mach 6.5. These investigations have used simple fuels (e.g., ethylene) as well as more complex liquid hydrocarbon fuels. Kay, et al.[1] conducted a series of hydrocarbon-fueled combustor experiments at Mach 5.6 conditions using ethylene and JP5. These studies demonstrated the viability of a piloted combustor operating in dual-mode. Another supersonic combustor concept developed by Siebenhaar, et al.[2] was explored at Mach 4 and 8 conditions using n-decane and a mixture of ethylene + n-decane, respectively. These experiments demonstrated the encouraging results that a fixed-geometry scramjet combustor could be effectively operated over a broad range of flight conditions. During the past ten years, the AFRL in-house research group has been exploring dual-mode scramjet combustors based on flush-wall fuel injection and cavity flameholders.[3-10] These studies examined ethylene and JP7-fueled combustor operability and performance and serve as the baseline for the flowpath development activities described in this paper.

Recent efforts have studied, or are planned to examine, hydrocarbon-fueled combustors in flight over a portion of the Mach 4 to 8 flight envelope. A sub-scale version of the liquid hydrocarbon-fueled Dual Combustor Ramjet (DCR) concept was flight-tested using the novel Freeflight Atmospheric Scramjet Test Technique (FASTT).[11] This flight test approach was developed as a means to quickly study scramjet-powered vehicles in a true flight environment for relatively low costs compared with full-scale flight testing. The X-51 program aims to demonstrate flight-weight, fuel-cooled, JP7-fueled scramjet combustors in flight over a range of Mach numbers from 4.5 to 6.5.[12-14] In contrast, the recent NASA X-43 flight experiments studied the characteristics of hydrogen-fueled scramjets at discrete Mach numbers of 7 and 10.[15] The Australian HyShot program[16] (and its recent follow-on efforts and the derivative program HYCAUSE[17]) explored various aspects of hydrogen-fueled supersonic combustion in flight typically at fixed Mach numbers between 8 and 10.

None of these experiments have or will investigate combustor mode transition and stable supersonic combustion of a hydrocarbon fuel at flight Mach numbers greater than 7. Combustor mode transition involves a change in combustor operation from that characterized as dual-mode, where a strong pre-combustion shock train is positioned upstream of the combustor, to scramjet-mode, where the pre-combustion shock train is absent leaving supersonic conditions (in a 1D sense) throughout the combustor. This change in mode is usually associated with an accelerating vehicle, although it may in

principle be accomplished at fixed flight conditions by reducing the overall equivalence ratio in the combustor or by tailoring the axial distribution of heat release in the combustor. Mode transition is difficult to study in ground-based facilities since most of these facilities operate at fixed Mach numbers. Sullins[18] reported results from a direct-connect study of a hydrogen-fueled supersonic combustor where the combustor inlet conditions were varied over a range of flight Mach numbers from 5.9 to 6.2. This variation in conditions was accomplished by increasing the stagnation temperature of the air stream entering the combustor at a constant Mach number set by a fixed-geometry facility nozzle. As conditions changed, the fuel-air equivalence ratio was held constant and the combustor experienced a transition from dual-mode to scramjet-mode operation. Combustor exit stream thrust was nearly constant during the transition.

HIFIRE HYDROCARBON-FUELED SUPERSONIC COMBUSTION EXPERIMENTS

The HIFiRE Program is a joint effort between AFRL and DSTO devoted to the study of basic hypersonic phenomena through flight experimentation. As part of this multi-flight program, experiments have been planned to explore the operating, performance, and stability characteristics of a simple hydrocarbon-fueled scramjet combustor. Objectives of these flight experiments include:

- Evaluate engine performance and operability through a dual-mode to scramjet-mode transition.
- Achieve Mach 8 combustion performance of $\phi_{B,4} \geq 0.7$ using a hydrocarbon fuel.
- Evaluate a gaseous fuel mixture as a surrogate for cracked liquid hydrocarbon fuel.
- Provide a test bed for diode laser-based instrumentation (water vapor and perhaps oxygen).
- Validate existing design tools for scramjet inlet, isolator, combustor, and nozzle components.
- Demonstrate a flight test approach that provides a variable Mach number flight corridor at nearly constant dynamic pressure.

Liquid hydrocarbon fuels are not considered for this experiment because the flowpath will not be actively cooled thereby making the challenge of vaporizing and/or cracking the liquid fuel prior to fuel injection quite difficult. Instead, a blend of two gaseous hydrocarbon fuels was sought to appropriately simulate the extinction characteristics of partially-cracked JP7. Colket and Spadaccini[19] described a blend of heptane/methane/ethylene that closely approximated the ignition delay characteristics of partially-cracked JP7. Pellett, et al.[20] characterized the laminar flame strength of this fuel mixture, along with several bi-component gaseous hydrocarbon fuel mixtures, in an opposed jet burner apparatus. In their initial work, results suggested that a volumetric mixture of 68% ethylene + 32% methane provided suitable agreement with the surrogate mixture results. After some refinement, Pellett, et al.[20] suggested that a volumetric mixture of 64% ethylene + 36% methane resulted in better agreement to the heptane/methane/ethylene mixture. This mixture of simple hydrocarbon fuels became the baseline fuel for the HIFiRE hydrocarbon-fueled supersonic combustion flight experiments.

This paper describes the development of an isolator/combustor flowpath for use in a hydrocarbon-fueled supersonic combustion flight experiment. The AFRL in-house baseline flowpath was studied using computational tools to better understand its suitability for the Mach 8 combustion experiment. The influences of various parameters were explored using ethylene as the combustor fuel. Following these simulations, an initial payload-integrated configuration was studied at Mach 8 conditions using both ethylene and a candidate fuel mixture. Finally, a refined configuration was examined over the range of anticipated flight conditions (Mach 6 – 8) using the baseline fuel mixture. A final flowpath was then selected for follow-on ground test evaluations to be conducted in the NASA Langley Research Center's Arc-Heated Scramjet Test Facility and for preliminary payload design activities.

FLOWPATH BACKGROUND

Recent investigations at AFRL were used to define the baseline isolator/combustor flowpath. Figure 1 shows a schematic of the initial flowpath; Table 1 contains the geometric details. This geometry includes a long, constant-area isolator with a cross-section of 38.1-mm (1.5-in.) x 101.6-mm (4.0-in.). The

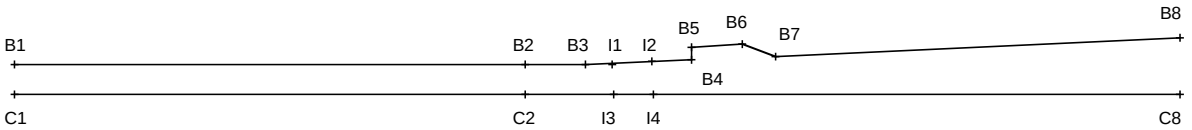

Figure 1. Baseline isolator/combustor flowpath schematic.

combustor has various fuel injection options and a cavity flameholder on the top wall that spans the entire flowpath width. The cavity depth is 17.1-mm (0.675-in.) and the aft wall angle is 22.5-deg. The four banks of fuel injectors shown in the schematic (I1, I2, I3, and I4) allow several variations to be explored. Each bank can be configured with either three or four injectors across the span (see Figure 2) and can be independently fueled. All injectors are inclined at 15-deg. to the flowpath wall and have the same diameter [3.2-mm (0.125-in.)]. The inner injectors are spaced 25.4-mm (1.0-in.) apart; the distance from the wall to the first injector is either 25.4-mm (1.0-in.) for the three-hole configuration or 12.7-mm (0.5-in.) for the four-hole configuration. The combustor top wall diverges at 2.6-deg. and the cowl wall is parallel to the flow direction. To date, this flowpath has been experimentally and computationally studied over a range of conditions simulating flight at Mach 3.5 – 5 using gaseous hydrocarbon fuels.[9,10]

CFD TOOL DESCRIPTIONS

VULCAN is a density-based CFD code applicable to complicated 2D and 3D geometries by using multiblock structured grids. Grid lines across a block interface can be continuous or discontinuous. The code solves the Reynolds-averaged Navier Stokes (RANS) equations appropriate for calorically or thermally perfect gases with a cell-centered finite volume scheme. The equation set can be integrated in a fully elliptic or space-marched manner. The inviscid fluxes can be evaluated with central differences, Roe's flux difference method, or a low-diffusion flux vector split scheme. Several flux limiters are provided to ensure total variation diminishing. A variety of two-equation turbulence models are available, along with one-equation and explicit algebraic Reynolds stress models. Assumed PDF options exist for modeling turbulence-chemistry interactions. Chemically reacting flows can be modeled with a general finite-rate kinetics model or a user specified function for chemistry. The code also contains full multi-grid capabilities, allowing rapid convergence for steady-state problems. For parallel computation, the MPI message passing library is used as a communication software in the code. Unless otherwise specified, the turbulence model was based on the Menter turbulence model in this study. The Menter model is essentially the standard high-Reynolds-number form of the Wilcox k-ω model near solid surfaces, but it smoothly transitions to a standard Jones-Launder k-ε model near the outer portion of the boundary layer and in regions of free shear. The turbulent Schmidt (Sc_t) and Prandtl (Pr_t) numbers control the modeled turbulent transport of mass and energy, respectively, and they were set to constant values. The value for Sc_t was calibrated to be 0.6 based on the comparison with experimental data and the value for Pr_t was selected to be 0.9. Chemical kinetics was initially modeled by a reduced mechanism developed based on

Table 1. Baseline isolator/combustor flowpath geometry.

	x [mm (in.)]	y [mm (in.)]
C1	0.000	0.000
C2	654 (25.750)	0.000
C8	1492 (58.750)	0.000
B1	0.000	38.1 (1.500)
B2	654 (25.750)	38.1 (1.500)
B3	730 (28.750)	38.1 (1.500)
B4	867 (34.144)	44.3 (1.745)
B5	866 (34.113)	61.4 (2.419)
B6	932 (36.681)	64.4 (2.536)
B7	974 (38.340)	49.1 (1.935)
B8	1492 (58.750)	72.7 (2.864)
I1	766 (30.166)	39.7 (1.564)
I2	817 (32.164)	42.0 (1.655)
I3	766 (30.168)	0.000
I4	817 (32.168)	0.000

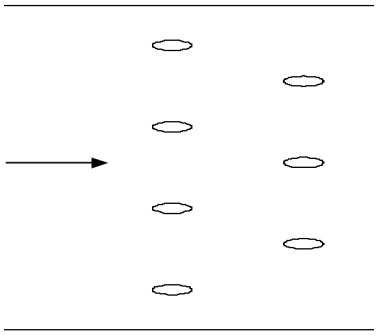

Figure 2. Four- and three-hole injector options.

the detailed mechanism of Qin et al.[21] and it was changed to the mechanism generated by Princeton University. The new mechanism consists of 22 species and it was developed based on the detailed mechanism of Wang and Laskin.[22]

Many simulations were performed using the CFD++ code, a general-purpose CFD tool developed by Metacomp Technologies.[23] CFD++ uses a finite-volume numerical framework, with multi-dimensional TVD schemes and Riemann solvers for accurate representation of supersonic flows. Multi-grid acceleration is available to provide a fast and accurate solution methodology for both steady and unsteady flows. A variety of one-, two-, and three-equation turbulence models are available for RANS calculations, along with large eddy simulation (LES) and hybrid RANS/LES options. Chemically reacting flows can be modeled with a general finite-rate kinetics model or a user specified function for chemistry. The code supports both structured (quadrilateral and hexahedral) and unstructured (triangle, prism, and tetrahedral) grids. MPI is used to take advantage of modern parallel-processing computers. CFD++ has several types of Riemann solver; the HLLC Riemann solver with Minmod flux limiting was used in the simulations described here. Unless otherwise specified, turbulence was modeled with the two-equation cubic k-ε model. This model has non-linear terms that account for normal-stress anisotropy, swirl and streamline curvature effects. At solid surfaces, an advanced two-layer wall function with the blended mode of equilibrium and non-equilibrium was employed to reduce grid requirements. Values of Sc_t and Pr_t were set to be the same as those in the VULCAN simulations. Chemical kinetics was modeled using the reduced kinetic mechanism generated by Princeton University (based on the detailed mechanism of Wang and Laskin[22]).

Three-dimensional CFD data were reduced to equivalent one-dimensional results using the separated-flow averaging technique. This method uses two distortion terms and results in the preservation of mass, momentum, and energy flows along with the pressure force and kinetic energy flow while introducing little artificial entropy gain. In this method, the projected areas (A_i), mass flow (W), momentum flows (mom_i), total energy flow (E), pressure force in each direction (PA_i), and kinetic energy flow (KE) are determined by integrating the CFD solution. Species mass fractions are then determined from the ratio of each species flow to the total mass flow. The static pressure is found using

$$P = \frac{\vec{PA} \cdot \vec{A}}{\vec{A} \cdot \vec{A}}.$$

The static enthalpy is determined from

$$h = \frac{E - KE}{W}.$$

The density, temperature, and entropy are then determined using the equation of state that was used in the CFD solver. Next, the velocity components are found using

$$u_i = \frac{mom_i - PA_i}{W} \quad for\ i = x, y, z.$$

Finally, the extra distortion terms are found using

$$\eta_a = \frac{W}{\rho\left(\vec{V} \cdot \vec{A}\right)},\ V_c = \frac{2KE}{W\left(\vec{V} \cdot \vec{V}\right)}.$$

Typically, the distortion terms remain near unity for non-separated flows. In these cases, the separated-flow averaging technique yields values that are very close to other averaging procedures. For separated flows like those encountered in shock trains and over cavity flameholders, the value of η_a decreases to mimic the actual flow area.

Burned equivalence ratio was computed at the combustor exit station using $\phi_{B,4} = \phi * \eta_{c,4}$. In this expression, the combustion efficiency at the combustor exit is computed based on static enthalpy change using

$$\eta_{c,4} = \frac{h\left(T_{ref}, Y_{i,4}\right) - h\left(T_{ref}, Y_{i,ref}\right)}{h\left(T_{ref}, Y_{i,ideal}\right) - h\left(T_{ref}, Y_{i,ref}\right)},$$

where the reference condition is at the isolator entrance and the ideal condition is determined from an equilibrium calculation using the static pressure and static enthalpy at the combustor exit station.

FLOWPATH DEVELOPMENT ACTIVITIES

During the initial phases of this effort, the configuration and overall size of the experimental payload were being studied in parallel with the development of the isolator/combustor flowpath. Both inward-turning and outward-turning inlet configurations were explored. These options would be integrated with either a combustor flowpath positioned along the centerline of the payload or a back-to-back flowpath configuration similar to HyShot[16] and HYCAUSE.[17] Prior to selecting a payload configuration, parametric studies were undertaken on the isolator/combustor flowpath to mature certain features of the design. After a candidate inlet and payload configuration were established, additional flowpath development occurred to assess the effects of integration on combustor operation and performance.

Also, during the early stages of this program, two flight experiments were envisioned. The first was to be devoted to the Mach 8 combustion goals, while the second would broaden the goals to include the dual-mode to scramjet-mode transition experiment. Due to financial constraints, the objectives of these two experiments were combined. This led to additional development of the inlet, which now was required to operate and provide adequate compression over a much broader Mach number range.[24] The isolator/combustor flowpath was validated using this new inlet configuration. The following discussion describes the evolution of the flowpath as the configuration and experimental requirements matured.

INITIAL PARAMETRIC INVESTIGATIONS

The VULCAN CFD code was used to simulate the baseline isolator/combustor flowpath at conditions representative of flight at Mach 8 conditions. Three-dimensional simulations were conducted using the geometry shown in Figure 1. Half of the flowpath was solved (centerline to sidewall). In these simulations, no specific inlet geometry existed, so plug flow was prescribed at the isolator entrance at conditions derived from preliminary studies of an inward-turning inlet [M_2 = 3.9, P_2 = 47.6 kPa (6.9 psia), and T_2 = 786 K]. The four-hole fuel injection configuration was used exclusively in these simulations, and ethylene was used as the fuel. The simulations included a partial nozzle attached to the combustor exit to ensure that the flow at the exit of the computational domain was supersonic and that the outflow boundary condition was well posed. Several parameters, including throat static pressure, fuel-air equivalence ratio, fuel injection site, combustor divergence angle, throat height, and wall boundary condition, were varied to better understand their influence on combustion performance and operability. Also, one case was studied to assess whether the cavity flameholder was required at Mach 8 conditions. Table 2 contains the details and key results from these studies (baseline case is shaded). To illustrate the parametric changes from case-to-case, modified parameters have been highlighted in red and italicized. Included in the table are results for the burned equivalence ratio at the combustor exit ($\phi_{B,4}$). In all cases, the combustor operated in scramjet-mode in that there was no pre-combustion shock train and the one-dimensional Mach number remained supersonic throughout the combustor flowpath.

Figure 3 presents plots of three-dimensional data resulting from simulations of Case 2. Local equivalence ratio, water mass fraction, and static temperature are shown. In these plots, the flow direction is from the lower left to the upper right. The top figure in each group shows the entire isolator/combustor flowpath while the lower figure shows the region around the fuel injectors and cavity flameholder. In Figure 3a, the stoichiometric surface appears as a white line in the various cross-sections shown. The cavity flameholder has entrained a substantial amount of fuel from the I1 injectors and is operating fuel rich. Downstream of the cavity flameholder, the fuel-air distribution becomes uniform across the combustor span, although variations in the vertical direction persist even at the combustor exit station.

Table 2. Parametric evaluations using baseline isolator/combustor flowpath.

Case	P_2 [kPa (psia)]	Wall BC	Fuel Site	ϕ	β (deg.)	h_2 [mm (in.)]	Cavity	$\phi_{B,4}$
1	*31.7 (4.6)*	Adiabatic	I1	1.0	2.6	38.1 (1.5)	Y	0.59
2	47.6 (6.9)	Adiabatic	I1	1.0	2.6	38.1 (1.5)	Y	0.56
3	*63.4 (9.2)*	Adiabatic	I1	1.0	2.6	38.1 (1.5)	Y	0.56
4	47.6 (6.9)	Adiabatic	I1	*0.7*	2.6	38.1 (1.5)	Y	0.39
5	47.6 (6.9)	*800 K*	I1	1.0	2.6	38.1 (1.5)	Y	0.65
6	47.6 (6.9)	Adiabatic	I1	1.0	2.6	38.1 (1.5)	*N*	0.51
7	47.6 (6.9)	Adiabatic	*I2*	1.0	2.6	38.1 (1.5)	Y	0.72
8	47.6 (6.9)	Adiabatic	*I0**	1.0	2.6	38.1 (1.5)	Y	0.51
9	47.6 (6.9)	Adiabatic	I1	1.0	2.6	*25.4 (1.0)*	Y	0.80
10	47.6 (6.9)	Adiabatic	I1	1.0	*1.5*	38.1 (1.5)	Y	0.78
11	47.6 (6.9)	Adiabatic	I1	1.0	*2.0*	38.1 (1.5)	Y	0.66
12**	47.6 (6.9)	Adiabatic	I1	1.0	2.6	38.1 (1.5)	Y	0.72
13**	47.6 (6.9)	*800 K*	I1	1.0	2.6	38.1 (1.5)	Y	0.64
14**	47.6 (6.9)	*800 K*	I2	1.0	2.6	38.1 (1.5)	Y	0.76
15**	47.6 (6.9)	*800 K*	I2	1.0	2.6	*25.4 (1.0)*	Y	0.86

*I0 was added to the computational grid 2-inches upstream of I1.
**Cases 12 – 15 used the VULCAN code with corrected wall function treatment.

The water mass fraction contours shown in Figure 3b indicate that combustion is occurring in the flameholder; no heat release is evident upstream of the cavity. A region of more intense water production occurs slightly downstream of the flameholder. This appears to be a result of the reflected cavity ramp shock interacting with the combustible fuel-air mixture in that region of the combustor, as observed in the static temperature data presented in Figure 3c.

Combustion performance results are summarized in Table 2. At the P_2 = 31.7 kPa (4.6 psia) condition (Case 1), combustion performance is slightly higher than for the baseline case due to a thicker boundary layer and its impacts to Mach number and static pressure. At the higher throat pressure condition (Case 3), the combustion efficiency does not change significantly from the baseline case. As the equivalence ratio is reduced from 1.0 to 0.7 (Case 4), the burned equivalence ratio decreases accordingly. Imposing an isothermal wall condition in Case 5 resulted in an increase in combustion efficiency compared with the baseline case that used an adiabatic wall condition. This trend was surprising and counterintuitive. After closer inspection and discussion with the VULCAN code developers, a bug was found that impacted the wall function treatment. Additional cases were run after the bug was corrected that produced the anticipated results (see Cases 12 and 13). Eliminating the cavity flameholder did not cause the combustor to extinguish, but it did significantly reduce the combustion performance as shown in the results from Case 6. Injector location plays an important role in combustor performance due to interactions with the cavity flameholder. Moving the fuel downstream to the I2 location results in a significant improvement in the burned equivalence ratio (Case 7). When the fuel injector location is moved upstream to the I0 location, mixing efficiency improves slightly, but combustion efficiency did not change substantially compared with the I1 location (Case 8).

Reducing the throat height improves the combustion performance compared with the baseline case by 43% (Case 9). Results from modifying the combustor divergence angle indicate that decreasing the divergence improves combustion performance compared with the baseline case. For the Mach 8 conditions, this reduction in combustor area ratio does not impact isolator operability. The 1.5-deg. divergence yields an increase in $\phi_{B,4}$ of approximately 40% while the 2.0-deg. case only improved the burned equivalence ratio by 18%. Together with the results from various injection sites, it appears that the parameters having the largest impact to combustor performance are fuel injection location (with I2 yielding the best performance) and throat height.

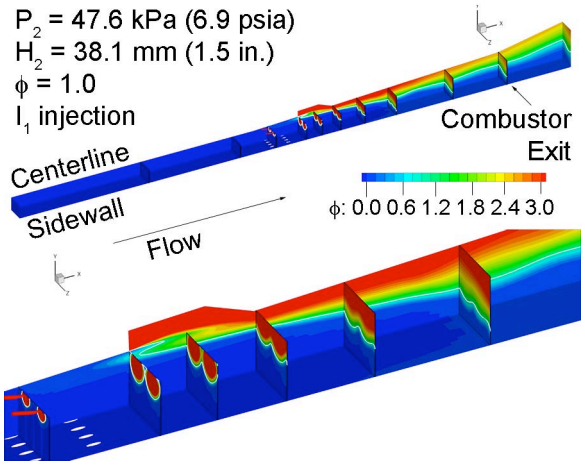

(a) Local equivalence ratio contours.

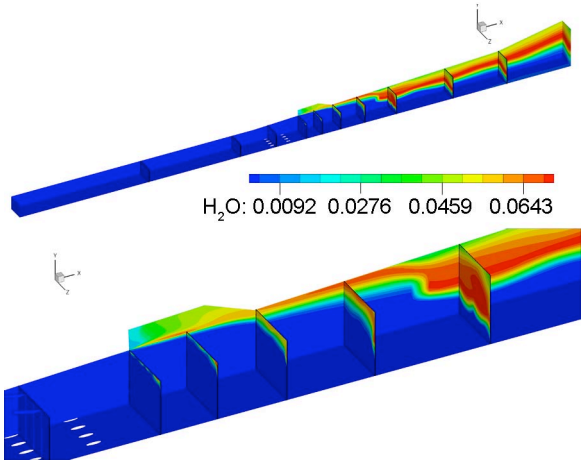

(b) Water mass fraction contours.

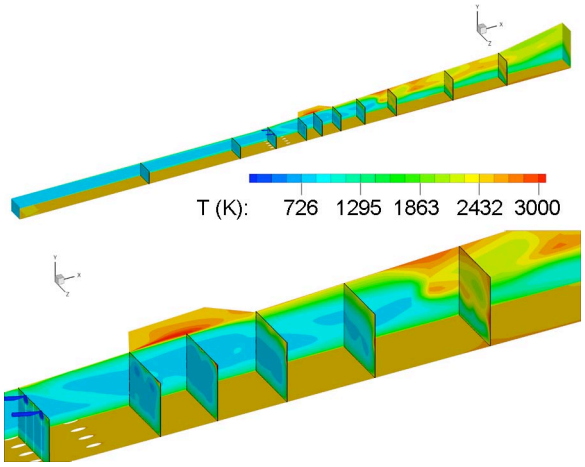

(c) Static temperature contours.

Figure 3. Contour plots from Case 2.

After correcting the wall function implementation, Cases 2 and 5 were re-computed to assess the impacts of the correction. The solution with adiabatic walls changed dramatically, but the isothermal wall solution changed only marginally. Figure 4 shows three-dimensional data from Case 12 for comparison with the original adiabatic wall solution shown in Figure 3. In general, higher levels of heat release are experienced after the wall function correction was implemented. This increases the combustor pressure and improves the fuel-air mixing. Figure 4a shows that the local equivalence ratio has become more uniform in the main portion of the combustor and the penetration of the stoichiometric surface has moved closer to the cowl wall in the vicinity of the cavity flameholder. The water mass fraction and temperature contours shown in Figure 4b and Figure 4c reveal evidence of combustion upstream of the flameholder and the body-to-sidewall interaction starting farther upstream. Table 2 compares the burned equivalence ratios predicted in Cases 2, 5, 12, and 13. In the adiabatic cases, $\phi_{B,4}$ increased from 0.56 to 0.72 while in the isothermal cases, the results were essentially equivalent.

Figure 5 and Figure 6 show results from simulations of Cases 14 and 15, respectively. These cases were also run with the corrected version of VULCAN and used the isothermal wall assumption. Two flowpath scales were used (h_2 in Case 14 is 38.1-mm (1.5-in.) while in Case 15, h_2 is 25.4-mm (1.0-in.)) and both cases used fuel injection from the I2 location. In both cases, the mixing and combustion performance have improved significantly compared with the corrected baseline simulation (Case 12). The local equivalence ratio distributions shown in Figure 5a and Figure 6a indicate that the fuel interacts with the sidewalls closer to the flameholder than shown in Case 12 and that the fuel mixture is closer to stoichiometric in these regions. This improves the flame propagation path from the flameholder around the combustor to the cowl side. Water is present even slightly upstream of the cavity in both cases (Figure 5b and Figure 6b) and high concentrations are found throughout the combustor. The flowfield in these cases is no longer uniform across the combustor span due to the substantial sidewall interaction that ultimately improves combustor performance. Static temperatures remain highest on the body side of the flowpath in Figure 5c and Figure 6c. Combustion performance, given by the burned equivalence ratio results shown in Table 2, suggests substantial improvement associated with the flowpath having the smaller throat height ($\phi_{B,4}$ in Case 15 is 0.86 compared with 0.76 in Case 14). Nevertheless, either flowpath configuration fueled using

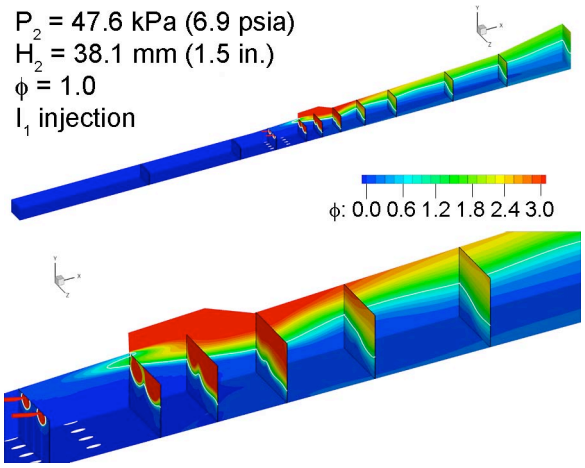

(a) Local equivalence ratio contours.

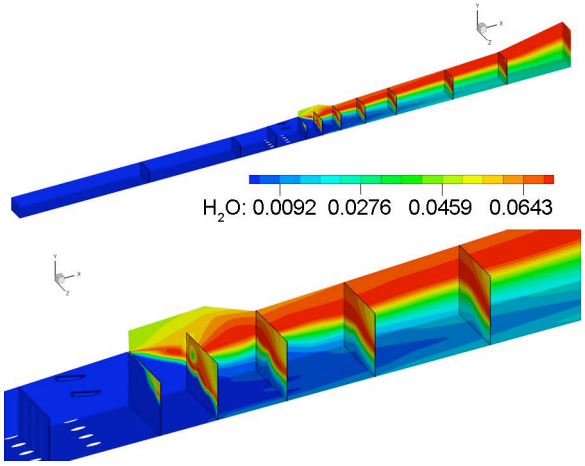

(b) Water mass fraction contours.

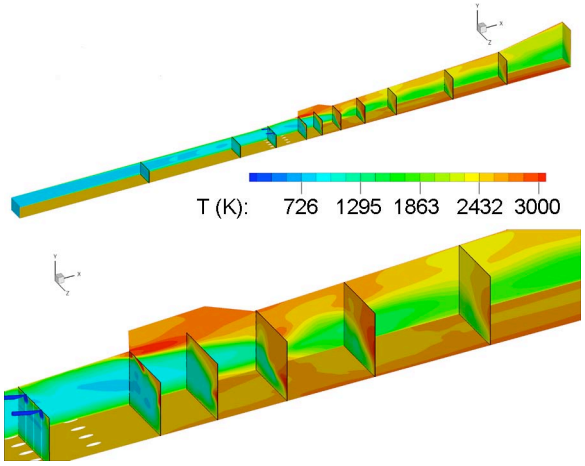

(c) Static temperature contours.

Figure 4. Contour plots from Case 12.

the I2 injection site at ϕ = 1.0 is predicted to exceed the performance goal of the Mach 8 experiment while operating in scramjet-mode.

At this point, two flowpath scales were analytically shown to meet or exceed the goals of the Mach 8 flight experiment. Absent from these simulations were the effects of inlet flow characteristics, payload integration (i.e., possible reductions in isolator and/or combustor length), and the desired fuel mixture. The next phase of simulations was planned to introduce these effects using a representative inward-turning inlet suitable for the Mach 8 combustion experiment and a 355.6-mm (14-in.) diameter payload configuration.

INITIAL PAYLOAD-INTEGRATED CONFIGURATION ANALYSES

Figure 7 shows the initial payload design configuration, which includes an inward-turning inlet, isolator/combustor, and bifurcated nozzle. A shroud contains the inlet until deployment near the test window. A bifurcated nozzle divides the exhaust stream at the vertical center of the flowpath and directs the exhaust out the top and bottom of the payload. A schematic of the baseline integrated isolator/combustor flowpath is shown in Figure 8a while geometric details are included in Table 3. The basic features of the flowpath did not change from the one shown in Figure 1, except that both isolator and combustor were truncated and the throat height was reduced to 25.4-mm (1.0-in.) based on the parametric studies and integration issues in this initial integrated configuration. The combustor divergence was split equally between the body and cowl sides (i.e., 1.3-deg. divergence on each side). Two banks of fuel injectors were retained from the original configuration (I2 and I4), as was the ability to use either the four-hole or the three-hole injector configuration (see Figure 2). Initially, only I2 was fueled using the four-hole injector configuration. Both ethylene and a volumetric mixture of 68% ethylene + 32% methane were studied.

Figure 8b shows a second flowpath configuration that was considered in these simulations. This alternative combustor added a duplicate flameholder to the cowl side while preserving all other features. This modification was incorporated to offset the potential effects of the reduced combustor length and the desired use of the hydrocarbon fuel mixture with a longer ignition delay time than pure ethylene. It also more effectively utilized the centerline flowpath configuration that allowed both body and cowl sides to be used for flameholding. The flowpath coordinates for this geometry are also included in Table 3.

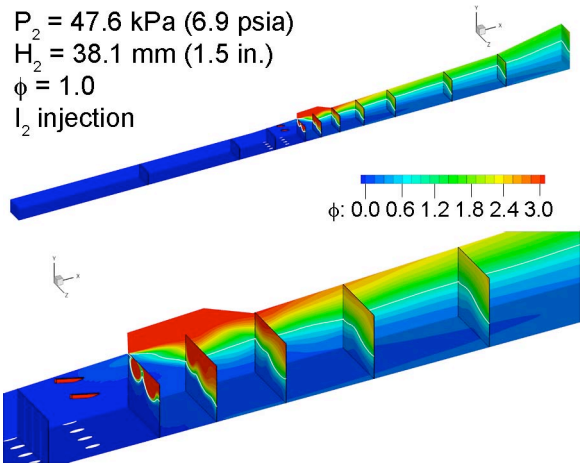

(a) Local equivalence ratio contours.

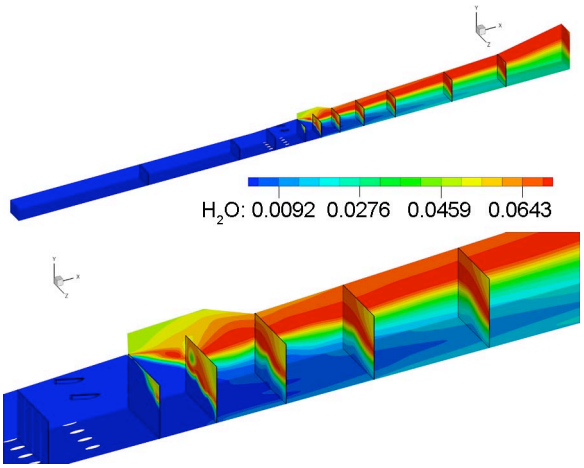

(b) Water mass fraction contours.

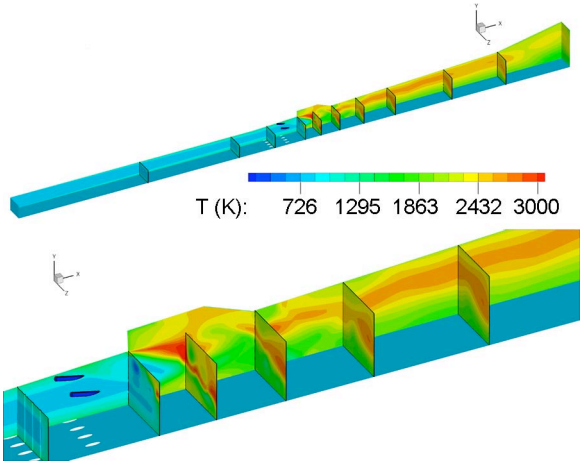

(c) Static temperature contours.

Figure 5. Contour plots from Case 14.

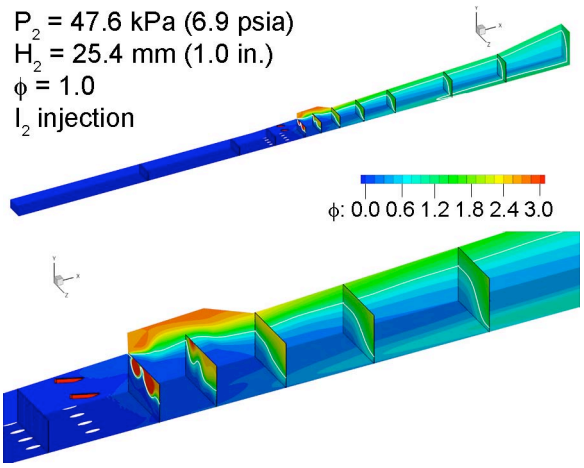

(a) Local equivalence ratio contours.

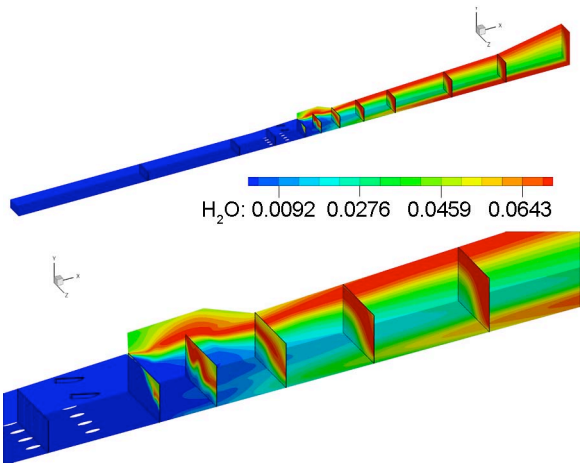

(b) Water mass fraction contours.

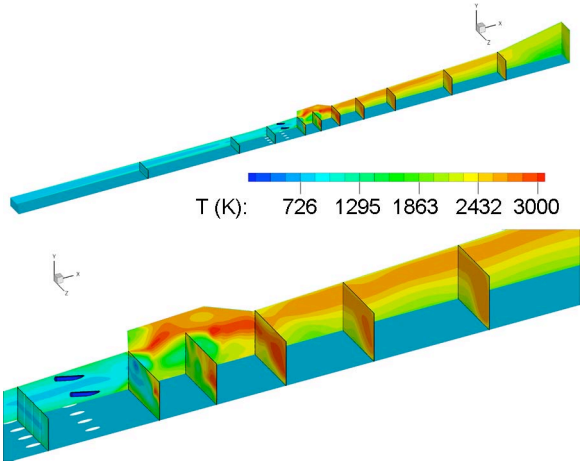

(c) Static temperature contours.

Figure 6. Contour plots from Case 15.

VULCAN was used for these simulations. Table 4 shows the details and results of the M_0 = 8, Q_0 = 71.8 kPa (1500 psf), α = 0 deg. simulations that were run to assess the performance of the flowpaths under the influences of both non-uniform inflow profile (as generated by the inward-turning inlet) and the two different hydrocarbon fuels. Cases 16 – 21 used the isothermal wall boundary

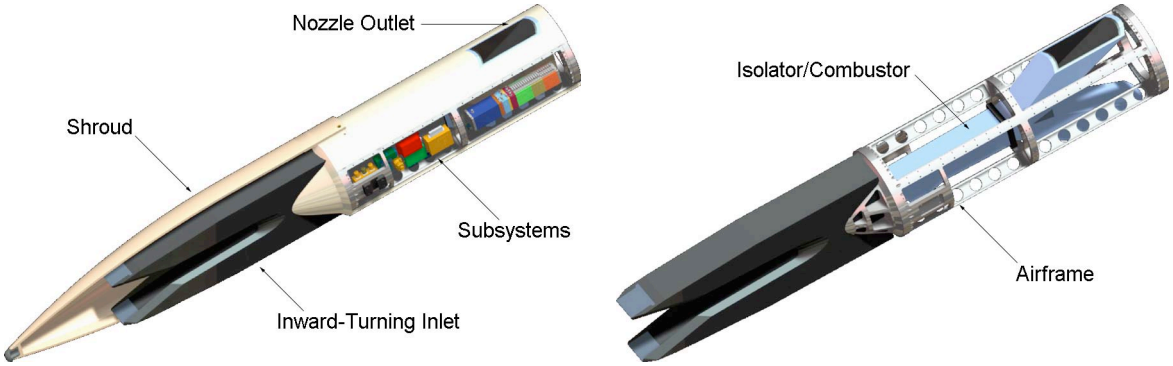

(a) View showing shroud and subsystems. **(b) View showing airframe and flowpath.**

Figure 7. Initial payload-integrated configuration.

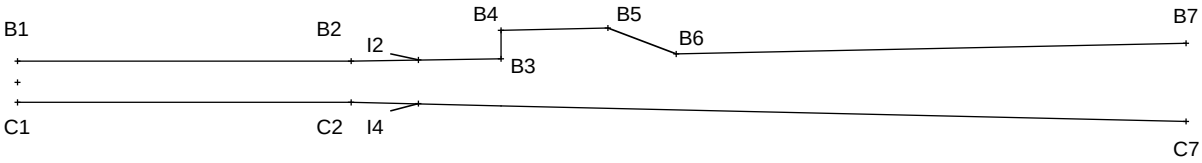

(a) Baseline integrated configuration.

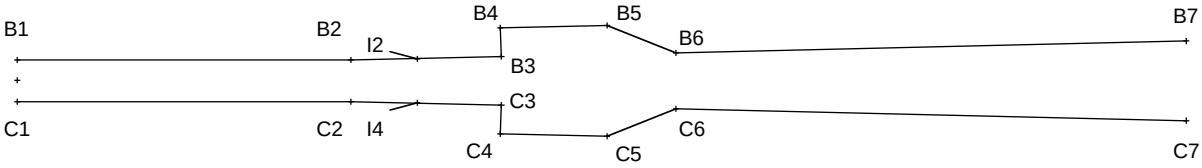

(b) Alternative integrated configuration.

Figure 8. Isolator/combustor flowpath schematics from the initial payload-integrated configuration.

conditions (800 K) and ϕ = 1.0. In Cases 16 and 17, all of the fuel was delivered through the I2 site. In Cases 18 and 19, the fuel was equally divided between the I2 and I4 sites. In Cases 20 and 21, the three-hole injector configuration was used in the I4 site. Thus, the fuel was divided between the I2 and I4 sites proportional to the fuel injector area – 60% (I2) and 40% (I4).

Figure 9 presents three-dimensional data from Case 17 using the baseline flowpath with body side injection and flameholding. Local equivalence ratio, water mass fraction, and static

Table 3. Isolator/combustor flowpath geometries in initial payload-integrated configuration.

	Baseline		Alternative	
	x [mm (in.)]	*y* [mm (in.)]	*x* [mm (in.)]	*y* [mm (in.)]
C1	0.000	-12.7 (-0.500)	0.000	-12.7 (-0.500)
C2	203 (8.000)	-12.7 (-0.500)	203 (8.000)	-12.7 (-0.500)
C3	-	-	295 (11.596)	-14.8 (-0.582)
C4	-	-	294 (11.581)	-31.9 (-1.256)
C5	-	-	359 (14.150)	-33.4 (-1.315)
C6	-	-	401 (15.794)	-17.2 (-0.677)
C7	711 (28.003)	-24.2 (-0.954)	711 (28.003)	-24.2 (-0.954)
B1	0.000	12.7 (0.500)	0.000	12.7 (0.500)
B2	203 (8.000)	12.7 (0.500)	203 (8.000)	12.7 (0.500)
B3	295 (11.596)	14.8 (0.582)	295 (11.596)	14.8 (0.582)
B4	294 (11.581)	31.9 (1.256)	294 (11.581)	31.9 (1.256)
B5	359 (14.150)	33.4 (1.315)	359 (14.150)	33.4 (1.315)
B6	401 (15.794)	17.2 (0.677)	401 (15.794)	17.2 (0.677)
B7	711 (28.003)	24.2 (0.954)	711 (28.003)	24.2 (0.954)
I2	244 (9.596)	13.6 (0.536)	244 (9.596)	13.6 (0.536)
I4	244 (9.596)	-13.6 (-0.536)	244 (9.596)	-13.6 (-0.536)

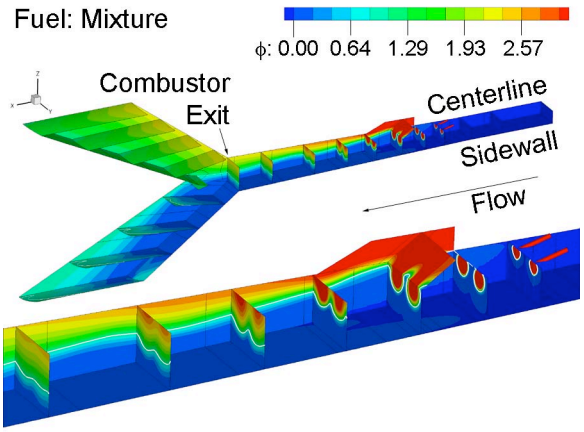

(a) Local equivalence ratio contours.

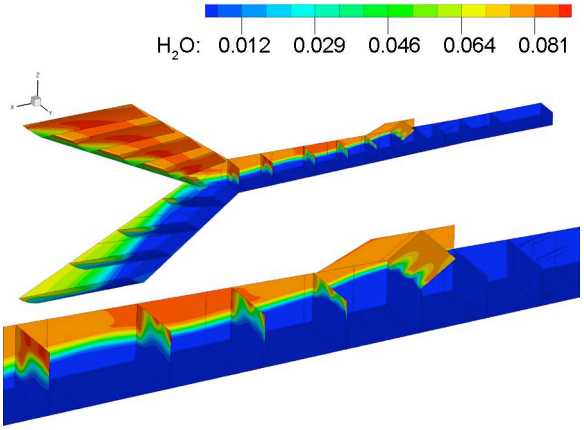

(b) Water mass fraction contours.

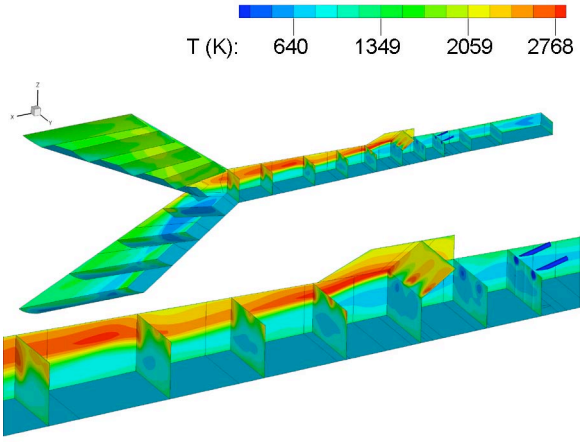

(c) Static temperature contours.

Figure 9. Contour plots from Case 17.

Table 4. Simulation details and results from initial payload-integrated configuration.

Case	Fuel Site	Fuel [C2H4 / CH4]	$\phi_{B,4}$
16	I2-4	100% / 0%	0.68
17	I2-4	68% / 32%	0.31
18	I2-4 / I4-4	100% / 0%	0.92
19	I2-4 / I4-4	68% / 32%	0.93
20	I2-4 / I4-3	100% / 0%	0.92
21	I2-4 / I4-3	68% / 32%	0.92

temperature contour plots are shown. In these plots, the flow direction is from the upper right to the lower left. The top figure in each group shows the entire flowpath while the lower figure shows the region around the fuel injectors and cavity flameholder. In Figure 9a, the stoichiometric surface appears as a white line in the various cross-sections shown. This surface progresses beyond the combustor mid-plane although movement of fuel to the cowl side is limited. Mixing effectiveness suffers due to the use of only body-side injectors and the truncated combustor (true regardless of the fuel selection). Water production is confined to the body side of the combustor as shown in Figure 9b, and the region of high combustor temperatures is confined on the body side (Figure 9c). The longer ignition delay time of the fuel mixture likely contributes to the poor heat release observed in Case 17 relative to the ethylene results from Case 16 (see Table 4). Both cases fall short of the desired combustion goal for the Mach 8 experiment (i.e., $\phi_{B,4} \geq 0.7$). The results in Figure 9 also reveal the potential for asymmetric loads to be generated on the payload as a result of the nozzle orientation.

Results from the alternative flowpath, which incorporates injection and flameholding on the body and cowl sides, show dramatically improved characteristics. Figure 10 contains three-dimensional data from Case 19 (fuel mixture). The local equivalence ratio plot (Figure 10a) reveals very desirable fuel-air ratios throughout the combustor and in both flameholders. Water production has increased significantly (Figure 10b) and the combustor temperatures shown in Figure 10c are substantially elevated compared with the results from the baseline geometry shown in Figure 9c. No evidence of a pre-combustion shock train is apparent despite the high levels of heat release near the cavity flameholders. These plots also indicate no significant asymmetries in the nozzle flowpaths. The performance results shown in Table 4 indicate burned equivalence ratios of 0.92 and 0.93 for the ethylene and fuel mixture cases, respectively.

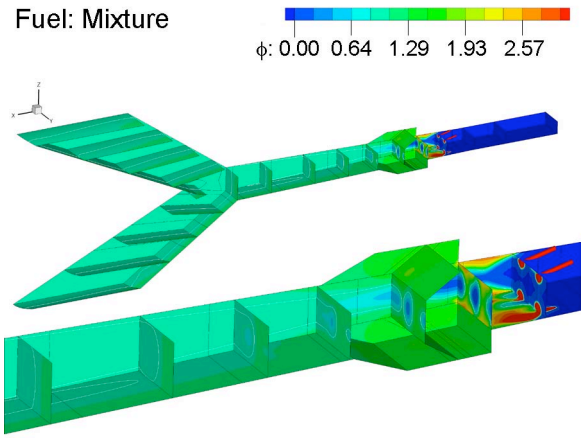

(a) Local equivalence ratio contours.

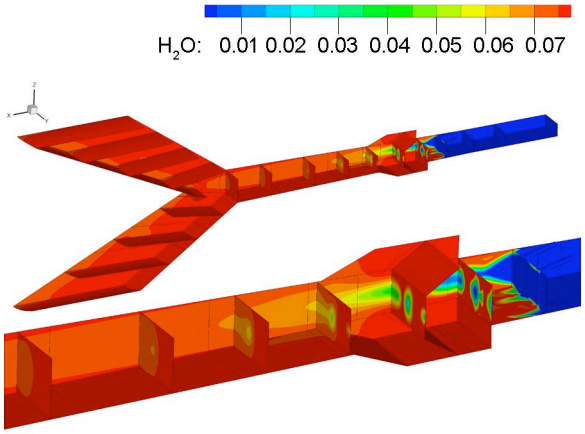

(b) Water mass fraction contours.

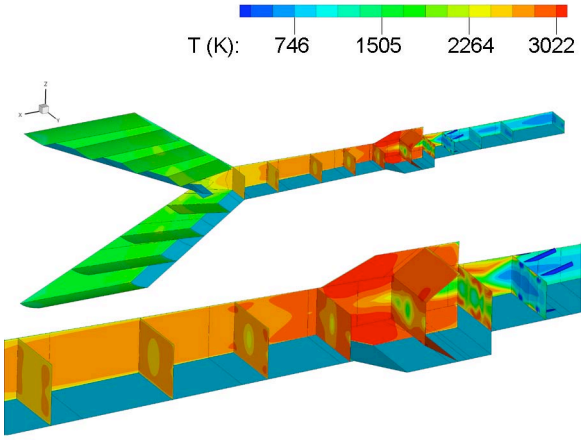

(c) Static temperature contours.

Figure 10. Contour plots from case 19.

When the I4 injection site is fueled with the three-hole configuration, no significant performance changes occur (burned equivalence ratios for both ethylene- and mixture-fueled simulations are both 0.92 as shown in Table 4). Slight asymmetries develop due to the asymmetric body-to-cowl fuel distribution, although much less significant than those shown in Figure 9.

Based on the results of these analyses, several conclusions were made. First, the alternative isolator/combustor flowpath was elevated as the new baseline flowpath because of its ability to overcome any detrimental influences of the shorter combustor and the use of the hydrocarbon fuel mixture. Second, symmetric fuel injection was selected as the baseline configuration, where both I2 and I4 injection sites would utilize the four-hole configuration. Since these sites are the primary injection sites and will be fueled together, they were designated P1. Third, as a means for mitigating the effects of any unforeseen flowfield asymmetries, the nozzle was rotated 90-degrees such that it divided the exhaust stream at the horizontal center and direct the exhaust gases out either side of the payload

ANALYSES OVER A BROADER MACH NUMBER RANGE

In support of the decision to combine the objectives of the Mach 8 supersonic combustion experiment with the dual-mode to scramjet-mode transition experiment, additional simulations were conducted over the range of flight Mach numbers from 6 – 8 to assess combustor operability and performance. These simulations were conducted with CFD++ using the results from the new forebody/inlet design[24] as inflow conditions for Mach 6, 7, and 8 analyses.

Figure 11 illustrates a conceptual design of the nominally 559-mm (22-in.) diameter payload that would be used to support the combined experimental objectives. Included in this sectioned view are the revised forebody/inlet, the two-piece shroud used to contain the inlet system during boost to the test window, the isolator/combustor, and the revised exhaust nozzle. The revised inlet geometry required that the payload diameter be increased from the previous version in order to achieve the desired compression over the Mach number range. In this concept, the isolator/combustor flowpath is identical to the alternative configuration described in Figure 8b and Table 3, except that secondary fuel injection sites were added on the body and cowl sides downstream of the cavity flameholders. It was felt that downstream injection might be required during dual-mode operation to ensure fueling at sufficiently high equivalence ratios while preserving a started inlet. These sites were located at (x, y) = [419-mm, ±17.6-mm (16.500-in., ±0.693-in.)]. The injectors were

oriented normal to the walls and had diameters of 2.4-mm (0.094-in.). Injector spacing was consistent with the four-hole configuration described in Figure 2. The secondary injection sites will be fueled together and are designated S1.

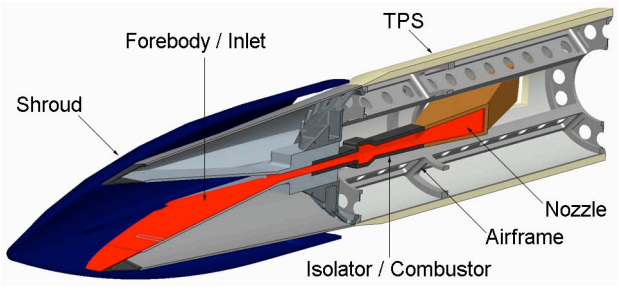

Figure 11. Conceptual design of revised payload supporting both mode transition and supersonic combustion performance objectives.

Figure 12 shows a notional fueling profile for the combined flight experiment. The diagram shows various events as functions of both Mach number and time from shroud separation. These data were derived from a nominal flight trajectory.[25] The new inlet is intended to start at or below Mach 5.5. Combustor ignition will occur at Mach 6 with the fuel distribution and total equivalence ratio being unknown. At this condition, the combustor will operate in dual-mode with the inlet started. As the payload accelerates following the ignition event, the equivalence ratio, and possibly the fuel distribution, will be adjusted such that started, dual-mode operation is maintained at the beginning of the mode transition experiment. At this point, the Mach number and equivalence ratio are unknown. During the mode transition experiment, changes in fuel distribution and equivalence ratio will not be made. This constraint is applied so that mode transition occurs naturally as the payload accelerates, rather than being forced by changes is the fueling arrangement. This implies that the fuel distribution and equivalence ratio at the start of the mode transition experiment be set consistent with what is required to meet the desired level of combustion performance at the Mach 8 scramjet-mode condition (i.e., $\phi_{B,4} \geq 0.7$). Based on previous simulations, it is expected that all fuel will be delivered using the P1 injectors at an equivalence ratio near unity at Mach 8. Thus, at the start of the mode transition experiment, these fueling conditions should also be achieved, but with a started inlet. These criteria will define the Mach number at the start of the mode transition experiment. If the flight trajectory allows acceleration beyond Mach 8, the fuel flow rate may be ramped down in an attempt to determine the lean operability limit of the combustor.

A series of CFD simulations was designed to provide some understanding of the combustor performance and operability along the nominal flight profile shown in Figure 13. Conditions and key results are included in Table 5 for the simulations conducted between Mach 6 and 8 (all conditions are at α = 0 deg.). Due to the inherent geometric symmetry of this configuration, one-quarter of the flowpath was modeled (quadrant defined by the vertical and horizontal centerlines and the body and side walls). Several cases were examined at the Mach 6 condition to assess the impacts of both equivalence ratio and fuel distribution. Fueling from P1 at ϕ = 1.0 was studied at Mach 7 and 8. In all cases, the final fuel mixture recommended by Pellett, et al.[20] was used (64% ethylene + 36% methane by volume) and the 800 K isothermal wall condition was imposed.

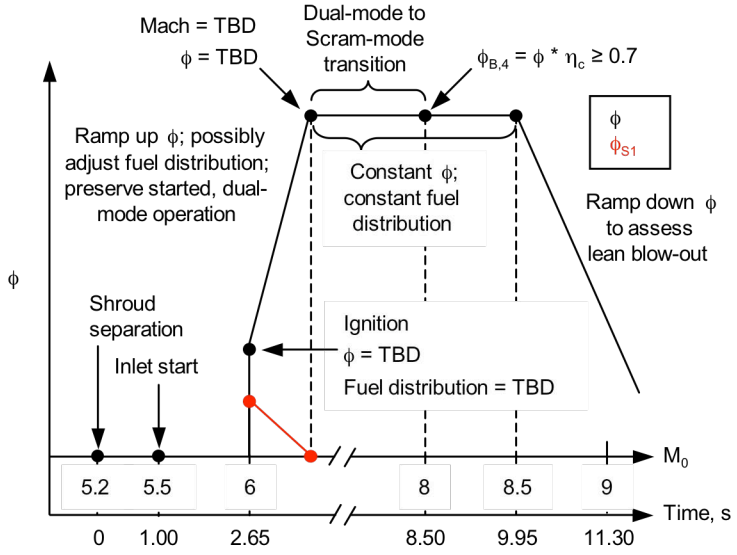

Figure 12. Notional fueling profile for flight experiment supporting both mode transition and supersonic combustion performance objectives.

Axial distributions of Mach number and static pressure

(normalized by throat static pressure) from the Mach 6 simulations are shown in Figure 14. In these plots, the isolator/combustor flowpath geometry and the axial positions of the P1 and S1 injector banks are included for reference. P1 injection cases are shown with symbols while P1 + S1 injection cases appear with solid and dashed lines. When using P1 injection, both $\phi = 0.5$ and 0.7 result in dual-mode operation with a started inlet. In these cases, the shock train resides in the downstream half of the isolator, and the 1D Mach number through the flameholder region is at or below sonic conditions. When secondary fuel injection is used to increase the total equivalence ratio to unity, additional heat release occurs downstream of the flameholders as evidenced by the reduced Mach number and increased static pressure downstream of $x = 419$ mm (16.5 in.). Secondary injection has only a slight impact on shock train position; in both cases, the shock train remains in the downstream half of the isolator and a started inlet is predicted. Combustion performance, as shown in Table 5, is quite high for the cases that use only P1 injection; however, in both of these cases, the burned equivalence ratio is below 0.7 ($\phi_{B,4} = 0.48$ and 0.64 for $\phi = 0.5$ and 0.7, respectively). The use of secondary injection results in increased values of $\phi_{B,4}$. Though $\phi_{B,4} \geq 0.7$ is not explicitly required at conditions below Mach 8, high values of burned equivalence ratio are desired to ensure realistic levels of heat release are occurring throughout the flight trajectory. Ultimately, practical considerations of weight and complexity will also influence the decision whether to incorporate secondary fuel injection into the payload design.

Table 5. Simulation details and results from revised payload-integrated configuration.

M_0	Q_0 kPa (psf)	ϕ	P1 (%)	S1 (%)	$\phi_{B,4}$	Mode*
6	87.0 (1817)	0.5	100	-	0.48	D
6	87.0 (1817)	0.7	100	-	0.64	D
6	87.0 (1817)	1.0	50	50	0.82	D
6	87.0 (1817)	1.0	70	30	0.82	D
7	82.8 (1730)	1.0	100	-	0.89	D
8	76.6 (1600)	1.0	100	-	0.96	S

*Mode: D = dual-mode, S = scramjet-mode

Similar one-dimensional results from the Mach 7 and Mach 8 simulation cases are shown in Figure 15. In these cases, the total equivalence ratio is unity and secondary injection is not used. The Mach 7 results show the pre-combustion shock train position being upstream of the P1 injection location and the 1D Mach number is near sonic or slightly subsonic through the flameholder region. Together, these features suggest that the combustor is operating in dual-mode in this simulation. At Mach 8, the pre-combustion pressure rise has moved downstream to near the P1 injection location and the Mach

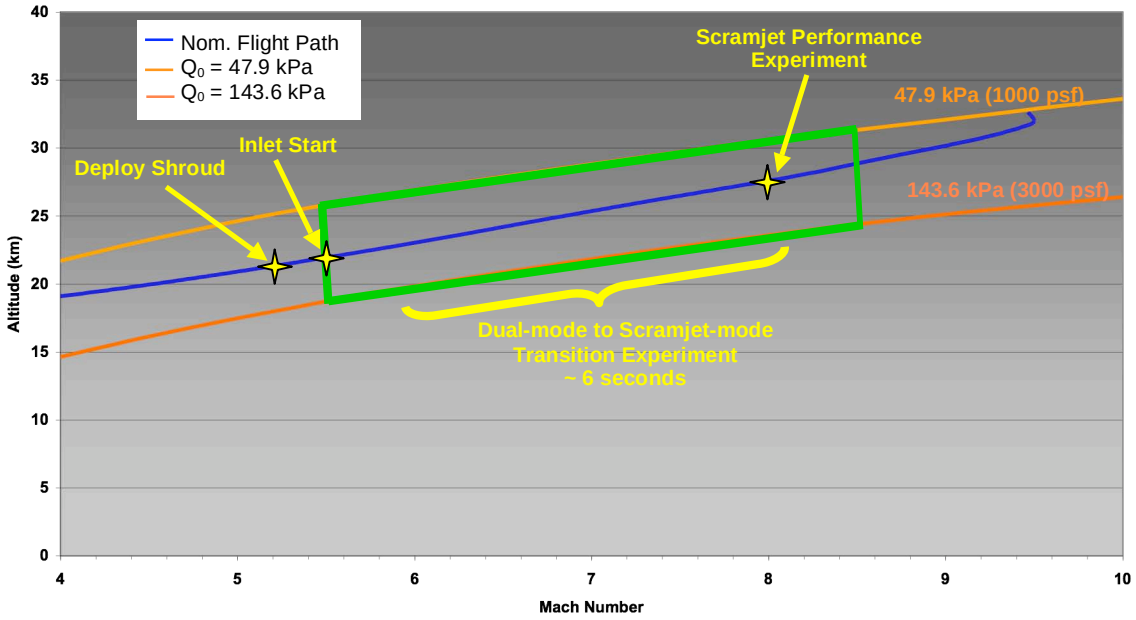

Figure 13. Nominal flight profile for the combined experiment.

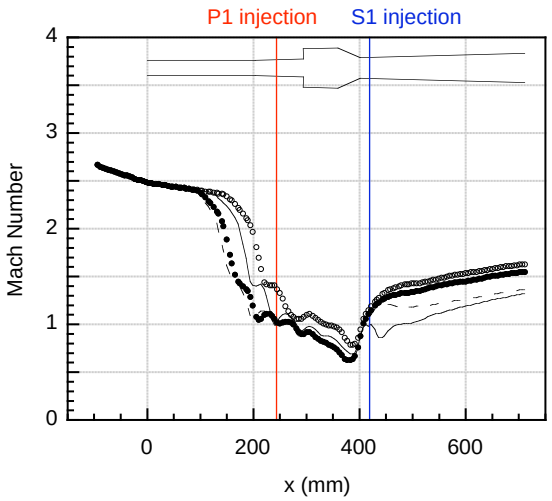

(a) Mach number.

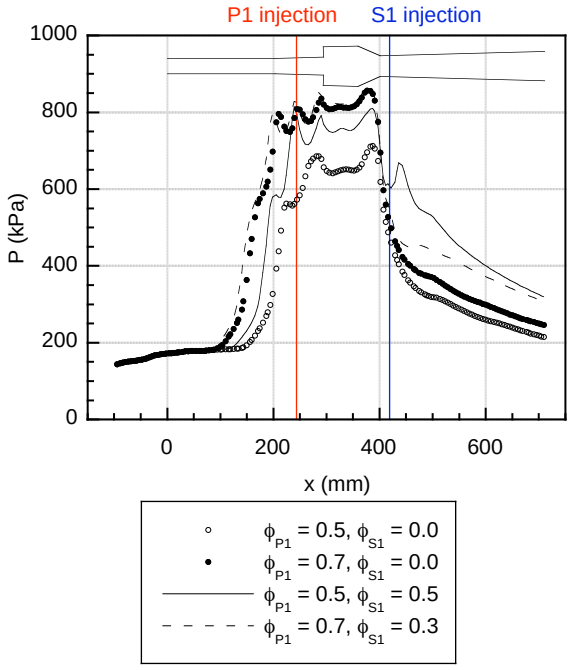

(b) Static pressure.

Figure 14. One-dimensional results from Mach 6 CFD simulations.

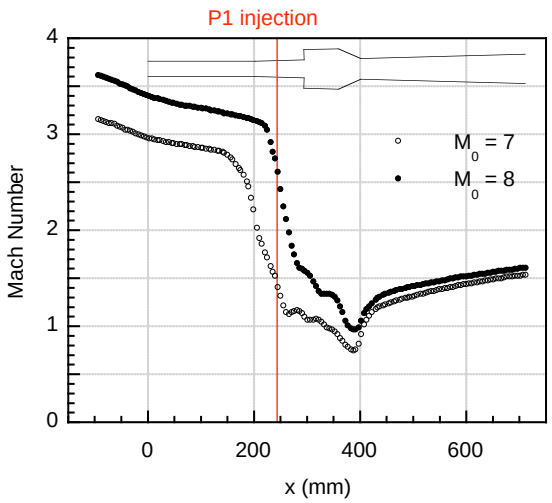

(a) Mach number.

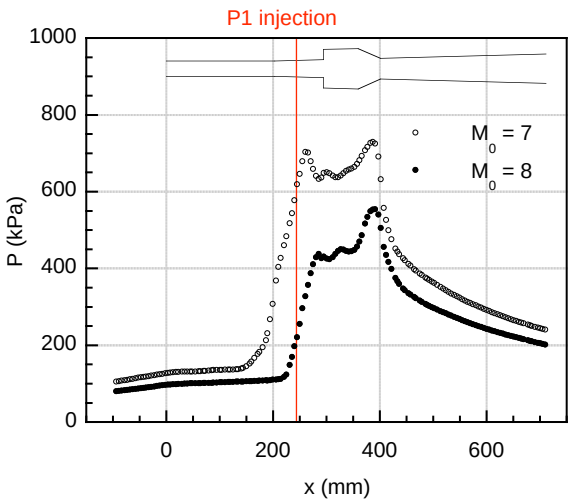

(b) Static pressure.

Figure 15. One-dimensional results from Mach 7 and Mach 8 CFD simulations.

number remains supersonic through the flameholder region except for a near-sonic condition at the cavity trailing edge. The small region of elevated pressure upstream of the P1 location is due to interactions in the corner regions of the flowpath. Based on these observations, the Mach 8 case appears to be operating in scramjet-mode (no strong separation regions upstream of injection and 1D Mach number is sonic or higher throughout the combustor). Combustion performance as shown in Table 5, exceeds the goal at both Mach 7 and Mach 8 conditions ($\phi_{B,4}$ = 0.89 and 0.96, respectively). Thus, it appears from these simulation results that mode transition will occur between Mach 7 and 8, though the actual start of the mode transition experiment is as yet unknown (speculation suggests that dual-mode operation with a started inlet will occur at flight conditions between Mach 6 and Mach 7 at ϕ = 1.0 with all fuel delivered from the P1 injection site).

SUMMARY

A hydrocarbon-fueled scramjet flight experiment has been planned as part of the HIFiRE Program. This experiment aims to study combustor mode transition and supersonic combustion performance in flight over a Mach number range from 6 to 8+. An isolator/combustor flowpath, based on an Air Force Research Laboratory in-house configuration, was matured for this experiment using three phases of computational simulations. An initial parametric study conducted at conditions representing Mach 8 flight revealed the influences of combustor geometry, fuel injection location, and wall boundary conditions using ethylene as the combustor fuel. These results guided the design of an initial integrated configuration using an inward-turning inlet concept. In this configuration, the isolator and combustor were truncated substantially to mange the overall payload length. Analyses of this integrated configuration revealed the benefits of modifying the combustor flowpath to be symmetric about the mid-plane. This modification improved combustion performance dramatically at the Mach 8 conditions using either ethylene or a mixture of ethylene and methane.

Following a re-design of the inlet system to accommodate broader Mach number operation, a revised integrated flowpath configuration was studied over the Mach 6 – 8 flight range. In this configuration, no changes were made to the isolator/combustor flowpath except the addition of secondary fuel injectors downstream of the cavity flameholders to potentially support dual-mode combustor operation. To date, the simulations of this configuration indicate that the experimental goals are achievable using a binary mixture of 64% ethylene and 36% methane, which is intended to be representative of partially-cracked JP7. At the Mach 6 ignition point, several fueling options were shown to allow dual-mode operation with a started inlet. The mode transition portion of the experiment will be conducted at constant fuel distribution and constant equivalence ratio. Using this approach, simulations suggest that the transition from dual-mode to scramjet-mode operation will occur between Mach 7 and 8 at $\phi = 1.0$ using the primary fuel injectors. Excellent combustion performance is predicted over the entire range of conditions. At Mach 8, the simulation results suggest that combustion performance exceeds the project goal of $\phi_{B,4} \geq 0.7$ with substantial margin.

ACKNOWLEDGEMENTS

The authors would like to acknowledge the HIFiRE Program for the opportunity to design and conduct experiments such as those described in this paper. The support of Parker Buckley and Robert Mercier of AFRL/RZA is greatly appreciated. Doug Davis of AFRL/RZAS developed the separated-flow averaging technique. Our partnership and interaction with NASA Langley Research Center personnel, specifically Neal Hass, Shelly Ferlemann, Andrea Storch, Paul Ferlemann, and Ken Rock, have been very valuable. We also appreciate Randy Voland's on-going involvement in this project. Finally, the efforts of Alan Drake and others at ATK were very helpful during the initial inlet design analyses.

REFERENCES

[1]Kay, I. W., Peschke, W. T., and Guile, R. N., "Hydrocarbon-Fueled Scramjet Combustor Investigation," Journal of Propulsion and Power, Vol. 8, No. 2, 1992, pp. 507-512.

[2]Siebenhaar, A., Bulman, M., Norris, R., and Thompson, M., "Development and Testing of the Aerojet Strutjet Combustor," AIAA Paper 99-4868, July 1999.

[3]Baurle, R. A., Mathur, T., Gruber, M. R., and Jackson, K. R., "A Numerical and Experimental Investigation of a Scramjet Combustor for Hypersonic Missile Applications," AIAA Paper 98-3121, July 1998.

[4]Mathur, T., Lin, K.-C., Kennedy, P. J., Gruber, M. R., Donbar, J. M., Jackson, T. A., and Billig, F. S., "Liquid JP-7 Combustion in a Scramjet Combustor," AIAA Paper 2000-3581, July 2000.

[5]Donbar, J. M., Gruber, M. R., Jackson, T. A., Carter, C. D., and Mathur, T., "OH Planar Laser-Induced Fluorescence Imaging in a Hydrocarbon-Fueled Scramjet Combustor," The 28th Symposium (International) on Combustion, The Combustion Institute, Pittsburgh, 2000, pp. 679-687.

[6]Gruber, M., Donbar, J., Jackson, T., Mathur, T., Eklund, D., and Billig, F., "Performance of an Aerodynamic Ramp Fuel Injector in a Scramjet Combustor," AIAA Paper 2000-3708, July 2000.
[7]Mathur, T., Gruber, M., Jackson, K., Donbar, J., Donaldson, W., Jackson, T., and Billig, F., "Supersonic Combustion Experiments with a Cavity-Based Fuel Injector," Journal of Propulsion and Power, Vol. 17, No. 6, 2001, pp. 1305-1312.
[8]Baurle, R. A., and Eklund, D. R., "Analysis of Dual-Mode Hydrocarbon Scramjet Operation at Mach 4-6.5," Journal of Propulsion and Power, Vol. 18, No. 5, 2002, pp. 990-1002.
[9]Lin, K.-C., Tam, C.-J., Boxx, I., Carter, C., Jackson, K., and Lindsey, M., "Flame Characteristics and Fuel Entrainment Inside a Cavity Flame Holder in a Scramjet Combustor," AIAA Paper 2007-5381, July 2007.
[10]Lin, K.-C., Jackson, K., Behadania, R., Jackson, T. A., Ma, F., Li, J., and Yang, V., "Acoustic Characterization of an Ethylene-Fueled Scramjet Combustor with a Recessed Cavity Flameholder," AIAA Paper 2007-5382, July 2007.
[11]Foelsche, R. O., Beckel, S. A., Betti, A. A., Wurst, G. T., Charletta, R. A., and Bakos, R. J., "Flight Results from a Program to Develop a Freeflight Atmospheric Scramjet Test Technique," AIAA Paper 2006-8119, December 2006.
[12]Boudreau, A. H., "Status of the U.S. Air Force HyTech Program," ISABE-2003-1170, September 2003.
[13]Norris, R. B., "Freejet Test of the AFRL HySET Scramjet Engine Model at Mach 6.5 and 4.5," AIAA Paper 2001-3196, July 2001.
[14]Mercier, R., and McClinton, C., "Hypersonic Propulsion - Transforming the Future of Flight," AIAA 2003-2732, July 2003.
[15]McClinton, C. R., "X-43-Scramjet Power Breaks the Hypersonic Barrier Dryden Lectureship in Research for 2006," AIAA Paper 2006-0001, Janaury 2006.
[16]Smart, M. K., Hass, N. E., and Paull, A., "Flight Data Analysis of the HyShot 2 Scramjet Flight Experiment," AIAA Journal, Vol. 44, No. 10, 2006, pp. 2366-2375.
[17]Walker, S. H., Rodgers, F. C., and Esposita, A. L., "Hypersonic Collaborative Australia/United States Experiment (HYCAUSE)," AIAA Paper 2005-3254, May 2005.
[18]Sullins, G. A., "Demonstration of Mode Transition in a Scramjet Combustor," Journal of Propulsion and Power, Vol. 9, No. 4, 1993, pp. 515-520.
[19]Colket, M. B., and Spadaccini, L. J., "Scramjet Fuels Autoignition Study," Journal of Propulsion and Power, Vol. 17, No. 2, 2001, pp. 315-323.
[20]Pellett, G. L., Vaden, S. N., and Wilson, L. G., "Opposed Jet Burner Extinction Limits: Simple Mixed Hydrocarbon Scramjet Fuels vs Air," AIAA Paper 2007-5664, July 2007.
[21]Qin, Z., Lissianski, V. V., Yang, H., Gardiner, W. C., Davis, S. G., and Wang, H., "Combustion Chemistry of Propane: A Case Study of Detailed Reaction Mechanism Optimization," The 28th Symposium (International) on Combustion, Pittsburgh, 2000, pp. 1663-1669.
[22]Wang, H., and Laskin, A., "A Comprehensive Kinetic Model of Ethylene and Acetylene Oxidation at High Temperature," Internal Report for an AFOSR New World Vista Program, 1998.
[23]Metacomp, http://www.metacomptech.com/index.html, 2006.
[24]Ferlemann, P., "Forebody and Inlet Design for the HIFiRE 2 Flight Test," 55th JANNAF Propulsion Meeting, Newton, MA, May 2008.
[25]Jackson, K. R., and Hass, N. E., "HIFiRE Flight 2 Scramjet Flight Experiment," 55th JANNAF Propulsion Meeting, Newton, MA, May 2008.